Cellulose (2015) 22:535–551
DOI 10.1007/s10570-014-0509-7

ORIGINAL PAPER

On the extraction of cellulose nanowhiskers from food by-products and their comparative reinforcing effect on a polyhydroxybutyrate-co-valerate polymer

Marta Martínez-Sanz · António A. Vicente · Nathalie Gontard · Amparo Lopez-Rubio · Jose M. Lagaron

Received: 20 May 2014 / Accepted: 15 November 2014 / Published online: 28 November 2014

Abstract The present work reports on the characterization of cellulose nanowhiskers (CNW) extracted from three different food by-products, i.e., wheat straw (WSCNW), Brewer's spent grains (BGCNW) and olive pomace (OPCNW), by using an optimized hydrolysis method similar to that developed to extract bacterial cellulose nanowhiskers (BCNW). WSCNW and BGCNW were seen to present optimal properties, with aspect ratio, crystallinity and thermal stability values comparable to those of BCNW. Additionally, the optimized hydrolysis treatment led to extraction yields higher than those previously reported for food by-products. The CNW were subsequently incorporated into a commercial polyhydroxybutyrate-co-valerate polymer (PHBV) by solution casting, and the produced nanocomposites were characterized. Although the addition of BGCNW and WSCNW was advantageous in terms of mechanical performance in comparison with OPCNW, no significant enhancement of the pure PHBV mechanical properties was reported because of the low nanofiller loadings used and the inherent difficulty of achieving a high degree of dispersion by the casting method. Interestingly, BGCNW and WSCNW presented reduced moisture sensitivity as compared with BCNW, leading to greater barrier performance and resulting in oxygen permeability reductions up to 26 % with WSCNW and 44 % with BGCNW.

Keywords Cellulose nanowhiskers · Food by-products · Polyhydroxyalkanoates · Nanocomposites · Barrier properties

M. Martínez-Sanz · A. Lopez-Rubio · J. M. Lagaron (✉)
Novel Materials and Nanotechnology Group, IATA, CSIC, Avda. Agustín Escardino, 7, 46980 Paterna, Valencia, Spain
e-mail: lagaron@iata.csic.es

A. A. Vicente
CEB – Centre of Biological Engineering, University of Minho, Campus de Gualtar, 4710-057 Braga, Portugal

N. Gontard
Agropolymers Engineering and Emerging Technologies, UMR 1208 IATE, UM2, CIRAD, INRA, Montpellier SupAgro, cc 023 Pl. E. Bataillon, 34095 Montpellier, France

Introduction

Cellulose is the main structural component from plant cell walls; thus, it is usually extracted from vegetal resources such as wood, cotton, hemp, etc. (Abe et al. 2007; Kargarzadeh et al. 2012; Morais et al. 2013; Satyamurthy et al. 2011). Additionally, cellulose can be synthesized by several bacterial species, which, in a static culture media rich in polysaccharides, are able to produce a highly hydrated pellicle of cellulose in the liquid/air interface (Iguchi et al. 2000). Although both plant and bacterial cellulose (BC) have the same chemical structure, consisting of a linear homopolysaccharide of poly-

β(1,4)-D-glucopyranoside chains linked by β-1-4-linkages, they are assembled differently into the distinct structural levels composing the macroscopic fibers. At the most basic structural level, cellulose chains are arranged in a highly ordered manner forming rod-like crystal units (Delmer and Amor 1995), known as cellulose nanocrystals or nanowhiskers. At the next structural level, cellulose nanowhiskers (CNW) are intercalated with disordered amorphous domains, forming cellulose microfibrils, which at the same time aggregate to form cellulose bundles or macrofibrils. Whereas pure cellulose bundles are produced in the case of BC (Martínez-Sanz et al. 2011b), cellulose microfibrils are found associated with other biopolymers, such as hemicelluloses, lignin and pectins in vegetal resources. Thus, several purification steps are required to isolate plant-derived cellulose (Lu and Hsieh 2012; Montaño-Leyva et al. 2011; Rahimi and Behrooz 2011).

The cellulose crystalline units or CNW are of particular interest in the development of nanocomposite materials due to their high crystallinity and aspect ratio. As demonstrated by numerous research works, the incorporation of CNW into polymeric materials may result in improved barrier and mechanical properties, provided that a good matrix-filler adhesion and high nanofiller dispersion are achieved (Capadona et al. 2009; Martínez-Sanz et al. 2012; Sanchez-Garcia and Lagaron 2010b; Ten et al. 2010). This approach is particularly interesting in the case of bio-based polymers, such as poly(lactic acid) (PLA) and polyhydroxyalkanoates (PHAs), which still present some lack of barrier and mechanical properties as compared to some benchmark petroleum-based polymers. Several works have reported on the production of polyhydroxybutyrate-co-valerate (PHBV) nanocomposites incorporating CNW with improved mechanical properties (Jiang et al. 2008; Ten et al. 2012). On the other hand, achieving significant barrier improvement has been shown to be more complicated because of the high moisture sensitivity of CNW (Martínez-Sanz et al. 2013b).

Regardless of the native cellulose source, the most widely used procedure for the extraction of CNW consists of a hydrolytic treatment with sulfuric acid, which produces a preferential digestion of the amorphous domains of the material (Rånby 1949). Following this procedure, CNW have been typically extracted from diverse vegetal resources (Abe et al. 2007; Kargarzadeh et al. 2012; Morais et al. 2013; Satyamurthy et al. 2011). More recently, the use of agroindustrial residues for the extraction of CNW is gaining attention because of their high availability and low price, being at the same time a strategy for waste valorization. Several by-products such as wheat straw (Rahimi and Behrooz 2011), sweet potato residue (Lu et al. 2013), coconut husk fibers (Rosa et al. 2010) and rice straw (Lu and Hsieh 2012) have been investigated as resources for the production of CNW. However, the extraction process applied in all these studies was similar to that typically used for the extraction of plant-derived CNW, leading to very low extractions yields of ca. 5 % (Lu and Hsieh 2012). An alternative procedure based on the combination of an extensive hydrolysis treatment with a subsequent neutralization step has been recently reported for the extraction of bacterial cellulose nanowhiskers (BCNW) (Martínez-Sanz et al. 2013a). As opposed to the traditional method, in which after a short hydrolysis time, the cellulose/acid suspension is centrifuged and CNW are extracted from the supernatant fraction, this alternative approach consists of the extraction of CNW from the precipitated fraction, thus producing thermally stable nanocrystals with extraction yields of up to 85 %.

In this work, three by-products, namely wheat straw, brewer's spent grains and olive pomace, which are generated in large amounts by the food industry (Montaño-Leyva et al. 2013; Mussatto 2014; Ramos et al. 2013), were used to produce CNW. Several purification steps were applied to isolate cellulose and a hydrolysis procedure similar to that previously reported for BC was utilized to increase the CNW extraction yields. The viability of these CNW was evaluated by comparing their properties and performance when incorporated into PHBV with that of the reference BCNW.

Materials and methods

Materials

The bacterial (PHA) was of melt-processable semi-crystalline grade purchased from Goodfellow Cambridge, Ltd. (UK) in pellets. This grade (from now on referred to as PHBV) consisted of a poly(3-hydroxybutyrate-co-3-hydroxyvalerate) polymer containing 12 mol % hydroxyvalerate plasticized with citric ester.

Fiber-based fractions obtained from different food by-products were used for the extraction of cellulose nanowhiskers. Durum wheat straw (WS), with a composition of 32.0 % cellulose, 20.5 % hemicellulose, 17.4 % lignin, 9.5 % extractives and 6.1 % ash, was supplied by INRA (Montpellier, France) and produced according to a previously described procedure (Silva et al. 2012). Brewer's spent grains (BG), with a composition of 35.8 % cellulose, 23.0 % lignin, 12.9 % hemicellulose, 1.8 % fat, 1.4 % protein and 1.0 % ash, were produced by the University of Minho (Braga, Portugal) by applying a double caustic treatment as previously described in the literature (Pires et al. 2012). Olive pomace fibers (OP), with a composition of 34.1 % lignin, 10.6 % hemicellulose and 7.8 % cellulose, were provided by the Fraunhofer Institute (Freising, Germany). BC pellicles synthesized by the procedure described in a previous work (Martínez-Sanz et al. 2011b) were used to produce the reference BCNW.

Sulfuric acid 96 %, toluene, ethanol 96 % (v/v), acetone 99.5 % and chloroform were purchased from Panreac (Barcelona, Spain).

Cellulose extraction from wheat straw (WS), Brewer's spent grains (BG) and olive pomace (OP)

In order to isolate cellulose from the different food by-products, a purification procedure, which has already been reported for various biomass sources (Abe et al. 2007; Lu and Hsieh 2012; Sun et al. 2004), was carried out.

To remove wax, pigments and oils, approximately 10 g of milled WS, BG or OP was subjected to Soxhlet extraction with 400 ml of toluene/ethanol 2:1 (v/v) during 24 h. The material was then oven dried at 60 °C overnight. Subsequently, to dissolve lignin, the de-waxed material was ground into powder and treated at 70 °C with 700 ml of 1.4 % $NaClO_2$ solution having a pH adjusted to 3–4. After 5 h the reaction was stopped by quenching with ice, and the excess liquid was decanted. The yellow solid was collected and washed with distilled water by vacuum filtration repeated until the filtrate became approximately neutral. The de-lignified material was then leached with 400 ml 5 % KOH solution for 24 h at room temperature, followed by 2 h at 90 °C, in order to remove the hemicellulose and silica. The material was separated by centrifugation at 12,000 rpm, 25 °C, for 10 min and subsequently washed several times with distilled water and separated by vacuum filtration until the filtrate became neutral.

Preparation of cellulose nanowhiskers

Cellulose nanowhiskers were extracted based on the optimized method reported for the production of BCNW (Martínez-Sanz et al. 2011a). This method consists of treating cellulose with 301 ml sulfuric acid/l water at 50 °C until most of the amorphous fraction has been digested. This is noticed by a sharp decrease in the viscosity of the cellulose/acid mixture, which shifts from a gel-like to a homogeneous liquid consistency. Extending the hydrolysis treatment after reaching this point has been seen to result in material degradation because of the digestion of the crystalline fraction. Therefore, the hydrolysis process had to be adapted to the properties of the different raw materials, i.e., depending on the crystallinity of the pure cellulose used as raw material. In the case of BCNW, a cellulose/acid ratio of approximately 7 g/l and hydrolysis time were applied, whereas milder conditions, i.e., a cellulose/acid ratio of 17 g/l and a hydrolysis time of 24 h, were required in the case of wheat straw CNW (WSCNW), brewer's spent grain CNW (BGCNW) and olive pomace CNW (OPCNW) to avoid cellulose degradation.

Following the acid hydrolysis, CNW were obtained as a white precipitate after several centrifugation and washing cycles at 12,500 rpm and 15 °C for 20 min. Subsequently, the material was re-suspended in deionized water and neutralized with sodium hydroxide until neutral pH and then centrifuged to obtain the final product as a partially hydrated precipitate. The humidity of the material was determined, and the yield of the extraction process was estimated.

Finally, the gel-like materials were solvent-exchanged into chloroform. The water of the partially hydrated precipitate was replaced by acetone by applying several centrifugation and re-dispersion cycles in which the supernatant was removed and replaced with acetone. After that, acetone was replaced by chloroform by subjecting the material to additional centrifugation cycles. The precipitate was collected and dispersed into chloroform by subjecting it to sonication during 10 min. The dry amount of

CNW was estimated, and the suspensions were kept refrigerated until use.

Preparation of PHBV-CNW nanocomposite films

Pure PHBV and nanocomposite films loaded with 1–2 % (w/w) CNW were prepared by means of solution casting using chloroform as the solvent. Solvent-exchanged BCNW, BGCNW, WSCNWs and OPCNW were dispersed into an adequate amount of chloroform by homogeneization (ULTRA-TURRAX) for 2 min, followed by sonication for 5 min. Subsequently, the required amount of PHBV was added to these suspensions, with a total solid content of 5 % (w/v), and stirred together at 40 °C during 2 h. Finally, the solutions were cast onto petri dishes, and films were attained after solvent evaporation at room temperature.

Scanning electron microscopy (SEM)

SEM was conducted on a Hitachi microscope (Hitachi S-4100) at an accelerating voltage of 10 kV and a working distance of 12-16 mm. PHBV and PHBV-CNW films cryofractured after immersion in liquid nitrogen were sputtered with a gold–palladium mixture under vacuum before their morphology was examined using SEM.

Transmission electron microscopy (TEM)

One drop (8 μl) of a 0.001 % aqueous suspension of CNW was allowed to dry on a carbon-coated grid (200 mesh). The crystals were stained with a 2 % (w/w) solution of uranyl acetate. TEM was performed using a JEOL 1010 equipped with a digital Bioscan (Gatan) image acquisition system at 80 kV.

Optical microscopy

Polarized light microscopy (PLM) examinations were performed using a Nikon Eclipse 90i optical microscope (IZASA, Spain) equipped with a 5-megapixel cooled digital color microphotography Nikon Digital Sight DS-5Mc camera. Captured images were analyzed and processed using Nis-Elements BR software (Nikon Instruments, Japan). To compare the different samples, all the films were imaged on their top surface.

FT-IR analysis

Raw BC, WS, BG and OP as well as purified cellulose extracts and the produced CNW were examined by FT-IR. Samples of ca. 2 mg were ground and dispersed in 200 mg of spectroscopic grade KBr. A pellet was then formed by compressing the sample at ca. 150 MPa. FT-IR experiments were recorded in transmission mode in a controlled chamber at 21 °C and 40 % relative humidity (RH) using Bruker FT-IR Tensor 37 (Rheinstetten, Germany) equipment. The spectra were taken at 1 cm^{-1} resolution averaging a minimum of ten scans. Analyses of the spectra were performed using Grams/AI 7.02 (Galactic Industries, Salem, NH, USA) software.

X-ray diffraction (XRD)

X-ray diffraction was carried out on a D5005 Bruker diffractometer. The instrument was equipped with a Cu tube and a secondary monochromator. The configuration of the equipment was θ–2θ, and the samples were examined over the angular range of 5°–45° with a step size of 0.02° and a count time of 4 s per point.

Peak fitting was carried out using the Igor software package (Wavemetrics, Lake Oswego, Oregon). Gaussian function was used to fit the experimental diffraction profiles obtained. For the fitting procedure, the reflections considered were (1) three at 14.8°, 16.4° and 22.5° 2θ (corresponding to the 1–10, 110 and 200 crystal planes, respectively) assigned to the cellulose I allomorph and (2) the amorphous halo centered at approximately 18.5° 2θ. The crystallinity index CI (XD) was determined by the method reported by Wang et al. (Wang et al. 2007):

$$\mathrm{CI}\ (\mathrm{XD}) = \frac{\sum A_{\mathrm{Crystal}}}{A_{\mathrm{Total}}} \times 100$$

where A_{Total} is the sum of the areas under all the diffraction peaks, and $\Sigma A_{\mathrm{Crystal}}$ is the sum of the areas corresponding to the crystalline peaks.

Differential scanning calorimetry (DSC)

Differential scanning calorimetry (DSC) of PHBV nanocomposites was performed on a Perkin-Elmer DSC 7 (PerkinElmer, Inc., USA) thermal analysis

system typically on 4 mg of dry material at a scanning rate of 10 °C/min from −30 °C to the melting point using N_2 as the purging gas. At least two specimens were measured for each sample. The first and second melting endotherms after controlled crystallization at 10 °C/min from the melt were analyzed. Before evaluation, similar runs of an empty pan were subtracted from the thermograms. The DSC equipment was calibrated using indium as a standard.

The crystallinity (%) of the PHBV was estimated from the corrected enthalpy for biopolymer content in the hybrid fibers, using the ratio between the enthalpy of the studied material and enthalpy of a perfect PHBV crystal, i.e., $X_C(\%) = \frac{\Delta H_f - \Delta H_c}{\Delta H_f^0} \times 100$ where ΔH_f is the enthalpy of fusion and ΔH_C the enthalpy of cold crystallization of the studied specimen, and ΔH_f^o is the enthalpy of fusion of a totally crystalline material. The ΔH_f^o used for this equation was 109 J/g for PHB (Scandola et al. 1997).

Thermogravimetric analyses (TGA)

Thermogravimetric (TG) curves were recorded with a Q500 TGA (TA Instruments, USA). The samples (ca. 20 mg) were heated from 50 to 600 °C with a heating rate of 10 °C/min under nitrogen atmosphere. Derivative TG curves (DTG) express the weight loss rate as a function of temperature.

Water vapor permeability (WVP)

Direct permeability to water was determined from the slope of the weight loss versus time curves at 24 °C. The films were sandwiched between the aluminium top (open O-ring) and bottom (deposit for the permeant) parts of a specifically designed permeability cell with screws. A Viton rubber O-ring was placed between the film and bottom part of the cell to enhance sealability. These permeability cells containing water as the permeant were then placed inside a desiccator at 0 % RH, and the solvent weight loss through a film area of 0.001 m^2 was monitored and plotted as a function of time. The samples were preconditioned at the testing conditions for 24 h, and to estimate the permeability values of the films, only the linear part of the weight loss data was used to ensure sample steady state conditions. The estimated slope values (expressed in g/h) were multiplied by the film average thickness (mm) and divided by water vapor pressure at 24 °C (atm) and the film area (m^2). The obtained values were then converted into the SI units kg m/(s m^2 Pa) by applying the appropriate conversion factor. Cells with aluminium films (with thickness of ca. 11 μm) were used as control samples to estimate solvent loss through the sealing. The lower limit of WVP detection of the permeation cells was of ca. 0.008 10^{-15} kg m/(s m^2 Pa) based on the weight loss measurements of the aluminium films. Water vapor weight loss was calculated as the total cell weight loss minus the loss through the sealing. The tests were done at least in duplicate.

Water uptake

The water uptake was estimated during the sorption experiments at 24 °C and 100 % RH by means of weight gain using a Voyager® V11140 analytical balance (Ohaus, USA). Thus, at saturation conditions, no changes in successive weight uptake were observed during the measurements of the specimens.

Solubility (S) was estimated from the water uptake at equilibrium, density of the materials and water vapor partial pressure at 24 °C. The diffusion coefficient of water (D) through the films was subsequently estimated from the solubility and permeability measurements, applying the following expression:

$$P = D \cdot S$$

Oxygen permeability

The oxygen permeability coefficient was derived from the oxygen transmission rate (OTR) measurements recorded using an Oxtran 100 equipment (Modern Control Inc., Minneapolis, MN, US). Experiments were carried out at 24 °C and 80 % RH, generated by a built-in gas bubbler and checked with a hygrometer placed at the exit of the detector. The samples were purged with nitrogen for a minimum of 20 h in the humidity-equilibrated samples, prior to exposure to an oxygen flow of 10 ml/min. A 5 cm^2 sample area was measured by using an in-house developed mask. Reduced sample areas while testing oxygen permeation in highly permeable materials enhance the reproducibility of the measurements, permit selecting defect-free areas and ensure minimum thickness variations.

Mechanical properties

Tensile tests were carried out at room conditions typically at 24 °C and 50 % RH on an Instron 4400 Universal Tester (Instron, USA). Preconditioned dumb-bell shaped specimens with initial gauge length of 25 mm and 5 mm in width were die-stamped from the films in the machine direction according to the ASTM D638. A fixed crosshead rate of 10 mm/min was utilized in all cases and results were taken as the average of at least four tests.

Statistical analysis

One-way analysis of the variance (ANOVA) was performed using the Statgraphics 5.1 software package. Comparisons between samples were evaluated using the Tukey test with a 5 % significance level.

Results and discussion

Characterization of the extracted CNW

During the first stage of this work, the extraction of CNW from three different food industry by-products (wheat straw, brewer's spent grains and olive pomace) was investigated. Additionally, BCNW were produced and used as a reference material to evaluate the properties of the food by-product CNW. Whereas no purification was required for BC, several treatments were required to isolate cellulose from the three different food by-products prior to the CNW extraction.

Table 1 gathers the yields corresponding to the overall extraction CNW process from the various raw materials as well as cellulose purification and acid hydrolysis yields. As observed, the most interesting material in terms of optimized overall CNW extraction yield was BC. This high extraction yield was a consequence of the high purity and crystallinity of the native material (Martínez-Sanz et al. 2011a) as well as the optimized hydrolytic treatment. The presence of impurities in the three different food by-products resulted in decreased CNW extraction yields, especially in the case of OP, which presented a very low cellulose extraction yield. However, it should be noted that the hydrolysis procedure applied in this work led to acid hydrolysis and overall WSCNW and BGCNW extraction yields similar to those reported for plant-derived CNW [22–51 % for CNW extracted from cotton; (Satyamurthy et al. 2011) and 23–59 % for CNW extracted from hemp (Kargarzadeh et al. 2012)] and much higher than those reported for CNWs extracted from food by-products [5–6 % for CNW extracted from rice straw (Lu and Hsieh 2012)]. Furthermore, CNW are obtained as diluted suspensions with the traditional hydrolysis method; thus, they are often subjected to a freeze-drying process, which is extremely detrimental to their subsequent dispersion into polymeric matrices. In contrast, CNW extracted in this work were obtained as much more concentrated gel-like materials which did not require any drying step.

Table 1 Extraction yields from bacterial cellulose, wheat straw, brewer's spent grains and olive pomace fibers

	Cellulose extraction yield (%)	Acid hydrolysis yield (%)	CNW extraction yield (%)
BC	–	76.9	76.9
WS	44.1	70.1	30.9
BG	60.0	50.7	30.2
OP	7.1	81.0	5.8

FT-IR analyses were carried out to investigate the structural and chemical effects of the applied extraction processes. Figure 1a displays the spectra of the native materials, whereas the spectra of the extracted CNW are shown in Fig. 1b. It is worth noting that, as deduced from Fig. 1a, while BC only presented bands characteristic for cellulose, additional bands corresponding to hemicellulose, lignin and silica could be detected for the three different food by-products. The removal of these additional components and isolation of cellulose were verified by the disappearance of the band located at 1,516 cm^{-1}, corresponding to vibrations of the aromatic ring of lignin (Lu and Hsieh 2012; Sun et al. 2005), the band at 1,729 cm^{-1}, corresponding to the esters and acetyl groups from hemicellulose (Sun et al. 2005) and the one appearing at 796 cm^{-1}, corresponding to the Si–O–Si stretching from silica (Lu and Hsieh 2012). On the other hand, from the spectra of the generated CNWs, some of the bands characteristic for cellulose, such as those located at 1,430, 1,375, 1,318, 1,165, 1,061, 1,034 and 900 cm^{-1} (Oh et al. 2005), presented narrower and higher intensity compared to the spectra of the purified

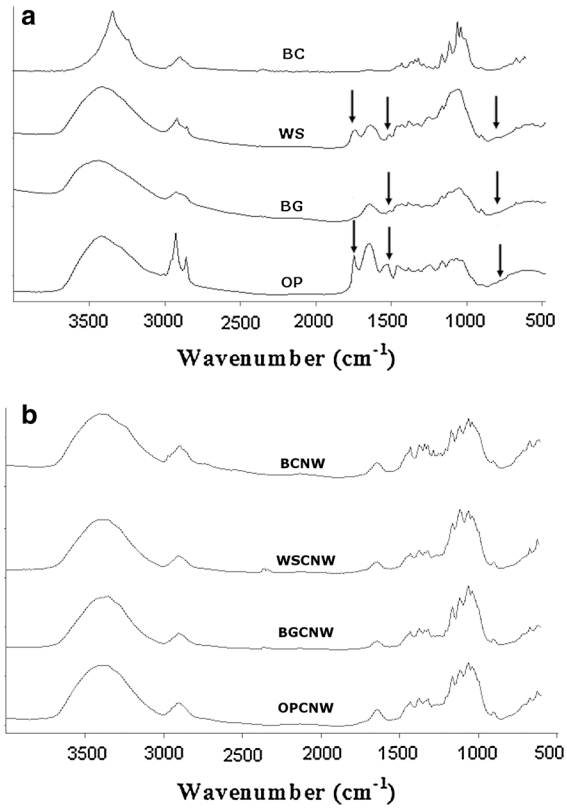

Fig. 1 FT-IR spectra of native cellulosic materials (**a**) and the extracted cellulose nanowhiskers (**b**). The arrows indicate the hemicellulose, lignin and silica characteristic peaks

cellulose extracts (spectra not shown), thus suggesting that the crystallinity of the cellulosic fraction was increased by means of the hydrolytic treatments. Furthermore, while BCNWs presented the bands assigned to both cellulose I_α (triclinic) and cellulose I_β (monoclinic) crystalline allomorphs, appearing at 750 and 710 cm^{-1}, respectively (Sugiyama et al. 1991), only the band assigned to cellulose I_β could be detected in the spectra of WSCNW, BGCNW and OPCNW. This supports the fact that while bacterial and plant-derived cellulose have the same chemical structure, they possess different structural organization.

The aspect ratio of CNW is an important parameter known to influence their reinforcing effect when incorporated into a polymeric matrix (Azizi Samir et al. 2005; Bras et al. 2011). Thus, the morphology of the different produced CNW was evaluated by estimating the CNW average length and cross-section from TEM micrographs of aqueous suspensions (cf. Fig. 2). From observation of Fig. 2 and Table 2, the native cellulose source used to extract the CNW affected mainly the cross section, while the CNW length was only significantly reduced in the case of OPCNW. As a result of their reduced cross section, BCNW presented the largest aspect ratio; thus, they would be expected to provide optimized mechanical performance when incorporated into PHBV (see "Morphological characterization" section). It is also worth noting that the CNW dimensions here reported differ significantly from those obtained by means of the traditional extraction method. For instance, a previous study in which WSCNW were produced by the typical hydrolysis approach, i.e., extracting the crystals from the supernatant, reported a length of 225 nm and width of 5 nm (Helbert et al. 1996), thus confirming that CNW dimensions are strongly affected by the hydrolysis procedure.

To estimate the crystallinity increase expected as a result of the purification and acid hydrolysis treatment, X-ray diffraction patterns of the different raw materials, i.e., before and after extraction of the CNW, were analyzed. As observed in Fig. 3, the crystalline structure of the cellulosic resources significantly differed. For BC three major diffraction peaks were observed at 14.5°, 16.4° and 22.5° 2θ, which are ascribed to the cellulose I crystallographic planes (1–10), (110) and (200), respectively [referenced to the cellulose I_β allomorph, according to the literature (French 2014)]. The diffraction patterns obtained for BG and WS corresponded to those previously reported for plant-derived cellulose (Bondeson et al. 2006; Elanthikkal et al. 2010), showing one major diffraction peak located at 22° 2θ and one shoulder in the region around 14–17° 2θ. This indicates, in agreement with the FT-IR results, that whereas BC is composed of a mixture of the cellulose I_α and I_β allomorphs, the I_β allomorph is predominant in the food by-product cellulose (Watanabe et al. 1998). The diffraction pattern of OP showed a wide amorphous halo, indicating that the amount of amorphous fraction was considerably high. A similar diffraction pattern was observed for untreated coconut fibers, and it was explained by their high lignin content (ca. 37 % lignin) (Rosa et al. 2010).

The estimated crystallinity indexes for the native materials were 79.1 ± 0.4 for BC, 67.1 ± 5.2 for BG, 45.4 ± 6.4 for WS and 30.8 ± 10.9 for OP. The crystallinity index seems to be linked to the cellulose

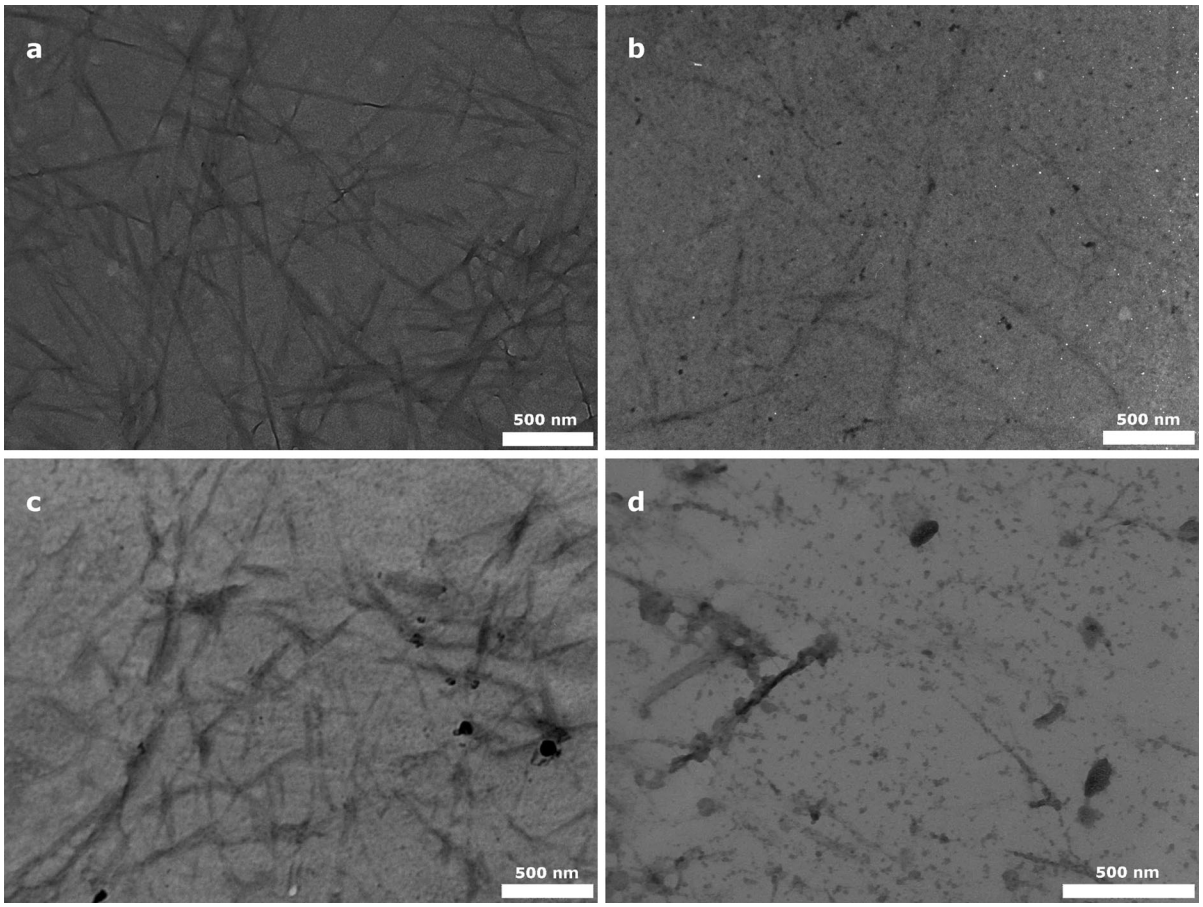

Fig. 2 TEM micrographs corresponding to CNW extracted from bacterial cellulose (**a**), wheat straw (**b**), brewer's spent grains (**c**) and olive pomace (**d**)

Table 2 Length, cross section and aspect ratio of CNW extracted from bacterial cellulose, wheat straw, brewer's spent grains and olive pomace fibers, estimated from TEM micrographs

	Length (nm)	Cross section (nm)	Average aspect ratio
BCNW	564.1 ± 228.2^{b}	16.9 ± 5.3^{a}	35.7 ± 9.5^{b}
WSCNW	574.1 ± 246.1^{b}	29.5 ± 9.8^{c}	25.8 ± 15.6^{ab}
BGCNW	515.0 ± 187.9^{b}	31.2 ± 8.7^{c}	21.6 ± 10.5^{a}
OPCNW	289.9 ± 97.5^{a}	21.7 ± 7.6^{b}	14.9 ± 8.3^{a}

Different superscripts within the same column indicate significant differences according to the ANOVA statistical analysis of the data ($p < 0.05$)

content found in the raw materials (cf. cellulose extraction yield in Table 1). After the acid hydrolysis, the crystallinity indexes increased up to 95.3 ± 0.3 for

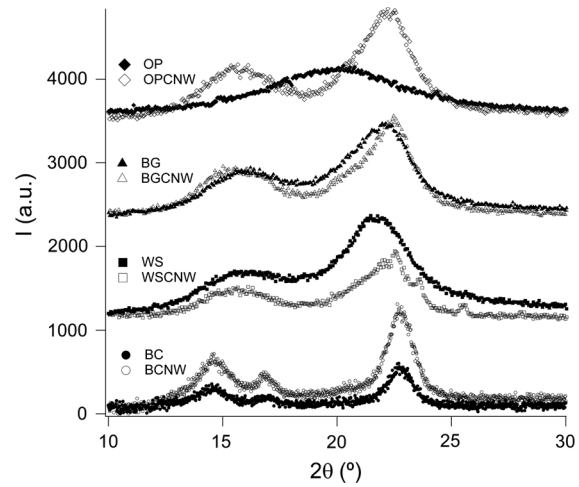

Fig. 3 X-ray diffraction patterns for the different cellulosic raw materials and extracted CNW

BCNW, 73.9 ± 1.5 for BGCNW, 78.3 ± 0.1 for WSCNW and 63.4 ± 6.1 for OPCNW.

Finally, the thermal stability of the extracted CNW was studied by TGA analyses, and the degradation profiles are displayed in Fig. 4. As observed, the thermal stability of the different materials was related to their crystallinity, the highly crystalline BCNW being the most thermally stable, whereas the less crystalline OPCNW were the most thermally unstable. While BCNW presented a one-step degradation profile, BGCNW, WSCNW and OPCNW exhibited two different degradation processes. The first degradation stage, taking place at temperatures between 250 and 350 °C, has been ascribed to cellulose degradation processes such as depolymerization, dehydration and decomposition of glycosyl units (Araki et al. 1998). On the other hand, the second degradation step, occurring at temperatures between 375 and 430 °C, has been previously attributed to the degradation of lignin (Montaño-Leyva et al. 2011; Sanchez-Silva et al. 2012). Thus, TGA results suggest that some residual lignin may still be present in the CNW extracted from the food by-products, although this residual amount should not be high, since the lignin characteristic peak was not detected in the FT-IR spectra of these CNW (cf. Fig. 1b).

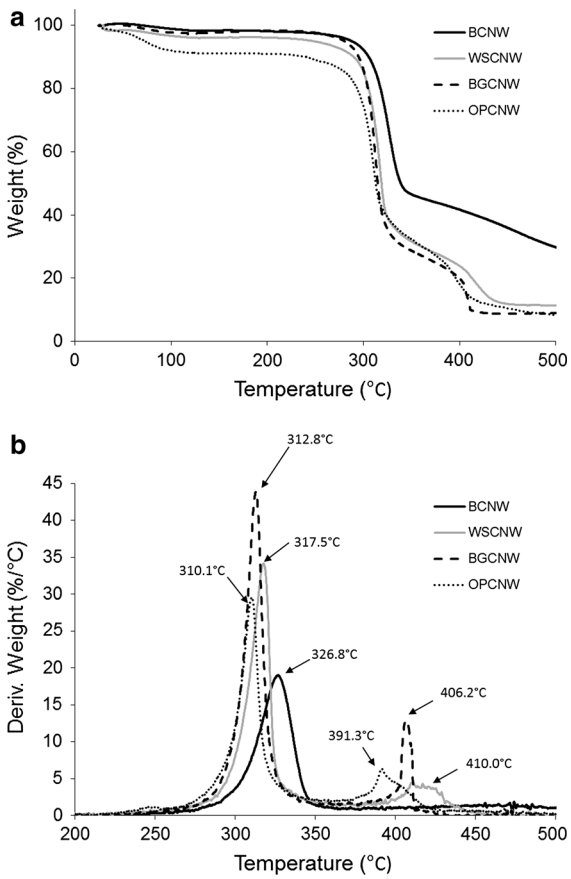

Fig. 4 (**a**) TG and (**b**) DTG curves of the different extracted CNW

To summarize, the extraction procedure applied in this work enabled the extraction of CNW from three different food industry by-products. BGCNW and WSCNW presented the most favorable properties, with relatively high extraction yields and good thermal stability, aspect ratios and crystallinity. However, BC is still the preferred source for the extraction of CNW due to the high purity of the native materials and the superior properties of the extracted BCNW.

Characterization of PHBV nanocomposites loaded with CNW

After extraction of CNW from different resources, these were incorporated into PHBV by solution casting. The differences found in the morphology, crystallinity and thermal stability of the produced CNW were expected to affect their performance when incorporated into the microbial biopolyester matrix. Thus, in what follows, the impact of incorporating the various CNW on the morphology, thermal, mechanical and barrier properties of PHBV nanocomposites was further investigated.

Morphological characterization

To confirm the different levels of nanofiller dispersion for all the prepared materials, their surface was first examined by optical microscopy (OM) with polarized light. The OM observations provide an indication of the distribution of the filler with particular attention to the presence of bigger aggregates. Representative pictures are shown in Fig. 5, where the CNW filler appears as bright areas within the matrix. These images suggest that a relatively good filler distribution was achieved for all the nanocomposites for 1 % (w/w) CNW loading, although it seemed that for BCNW the dispersion was improved as compared to the other materials. In addition, when the nanofiller concentration was further increased up to 2 % (w/w), a significant agglomeration effect could be detected for the samples loaded with WSCNW and OPCNW.

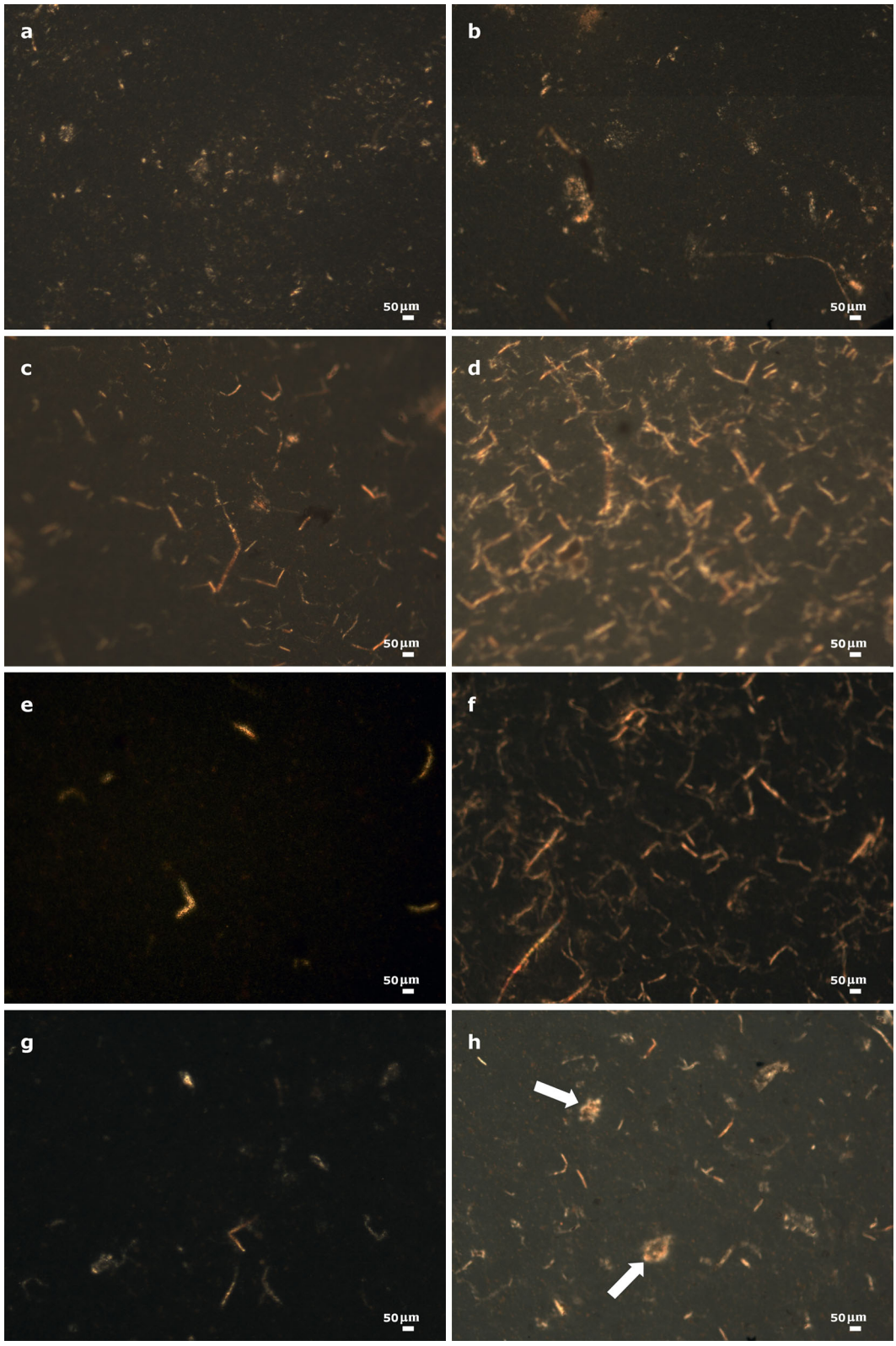
a
50 µm
b
50 µm
c
50 µm
d
50 µm
e
50 µm
f
50 µm
g
50 µm
h
50 µm

◀**Fig. 5** Polarized light optical microscopy images of PHBV nanocomposite films containing (**a**) 1 % (w/w) BCNW, (**b**) 2 % (w/w) BCNW, (**c**) 1 % (w/w) WSCNW, (**d**) 2 % (w/w) WSCNW, (**e**) 1 % (w/w) BGCNW, (**f**) 2 % (w/w) BGCNW, (**g**) 1 % (w/w) OPCNW and (**h**) 2 % (w/w) OPCNW. The *arrows* indicate CNW agglomerates

To further analyze the distribution of the CNW filler in the nanocomposites in the micron and submicron range, cryo-fractured sections of the developed films were studied by SEM and representative pictures are shown in Fig. 6. The pure polymer presented a rough fracture surface, which has been previously observed for PHBV casting films (Garrido et al. 2011). For the nanocomposite films, CNW appeared in the micrographs as bright white areas, similarly as reported for PHBV-BCNW nanocomposites produced by casting (Martínez-Sanz et al. 2013b). From observation of the micrographs, it seems that BCNW and BGCNW presented the highest degree of dispersion, whereas for WSCNW and OPCNW some larger aggregates were identified within the fractured surfaces. Agglomeration was also promoted by increasing the nanofiller concentration, this effect being more evident for WSCNW- and OPCNW-loaded nanocomposites. A certain degree of agglomeration was also reported when increasing the loadings of BCNW in PHBV nanocomposites produced by casting (Martínez-Sanz et al. 2013b). Achieving an optimal CNW dispersion is one of the main issues when preparing CNW-loaded nanocomposites, and several strategies, such as surface modification, electrohydrodynamic processing, etc., have been reported in the literature (Martínez-Sanz et al. 2014). In this sense, the casting method is not expected to provide the most optimal CNW dispersion because of the inherent difficulty of properly dispersing CNW in organic solvents.

Thermal properties and thermal stability

With the aim of investigating the effect of the incorporation of the different CNW in the thermal properties of the PHBV nanocomposites, DSC analyses of all the samples were carried out, and the results are summarized in Table 3. The melting temperatures (T_{m1} and T_{m2}) and corresponding melting enthalpy (ΔH_{m1} and ΔH_{m2}) normalized to the PHBV content of the nanocomposite films were obtained from the DSC first heating run, whereas the glass transition temperature was determined from the second heating run (T_{g2}). As deduced from the results, the PHBV grade used through this work (with 12 % valerate content) presented two melting steps, just as reported in previous works (Jiang et al. 2008; Sanchez-Garcia et al. 2008; Ten et al. 2010). This behavior has been explained by the fact that more defective or smaller crystals melted and subsequently recrystallized, forming more perfect crystals, which melted at higher temperature (Jiang et al. 2008; Ten et al. 2010).

In general, the thermal properties of PHBV were not strongly affected by the incorporation of CNW. Although the differences were not statistically significant, there seems to be an overall trend of decreased crystallization temperature and slightly higher glass transition temperature with the addition of CNW. The increase of T_g, which implies constrained mobility of the amorphous PHBV chains, has been shown to be conditioned by achieving a relatively good CNW dispersion (Martínez-Sanz et al. 2013b; Ten et al. 2012). Interestingly, the nanocomposites with 1 % BCNW, 1 % WSCNW and 1 % BGCNW, i.e., those loaded with the highest aspect ratio CNW and with optimized dispersion, presented a more obvious effect in the T_g. The presumably lower T_C observed for the nanocomposites as compared with pure PHBV suggested that the CNW somehow hindered the crystallization process of PHBV upon cooling. This observation further supports the fact that dispersed CNW restrict the mobility of the PHBV amorphous chains, hence interfering in the crystallization process.

Thermogravimetric analyses were carried out in order to study the effect of CNW incorporation on the thermal stability of the produced nanocomposites, and the estimated parameters are gathered in Table 4. The first thing worth noting is that the pure polymeric matrix possessed similar or even lower thermal stability than the CNW, as deduced by comparing the parameters given in Table 4 to the TGA analyses shown in Fig. 4. The degradation temperature of the PHBV used in the present work was lower than that previously reported for several PHBV grades (Martínez-Sanz et al. 2013b), probably as a consequence of the plasticizer present in this commercial grade. In agreement with previous works (Martínez-Sanz et al. 2013b; Yu et al. 2012), the addition of CNW had a positive impact on the thermal stability. This has been attributed to the suppression of the six-membered ring ester formed during the first degradation steps of

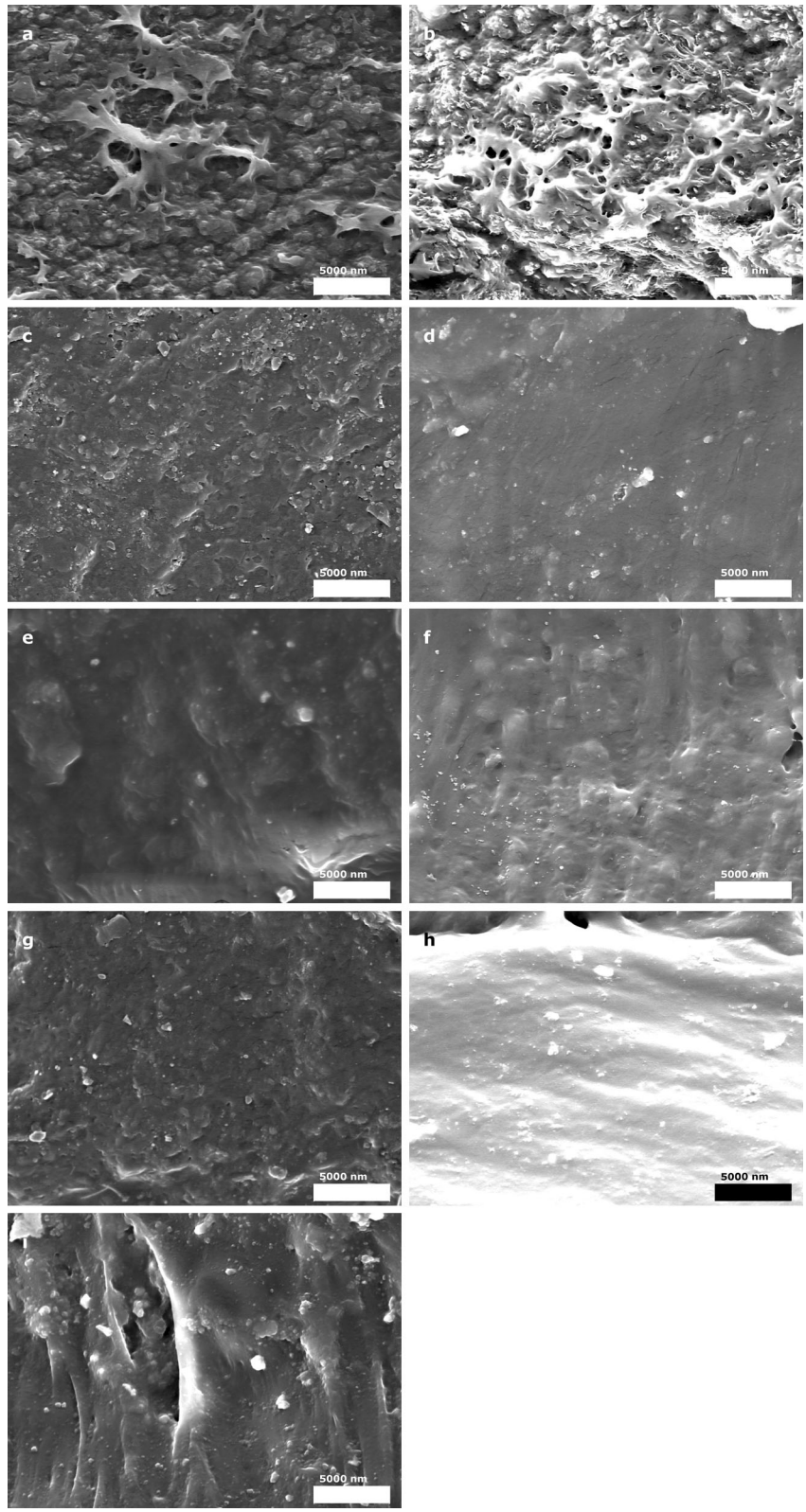

Fig. 6 SEM micrographs of the cryofractured section obtained from PHBV nanocomposite films: (a) pure PHBV, (b) 1 % (w/w) BCNW, (c) 2 % (w/w) BCNW, (d) 1 % (w/w) WSCNW, (e) 2 % (w/w) WSCNW, (f) 1 % (w/w) BGCNW, (g) 2 % (w/w) BGCNW, (h) 1 % (w/w) OPCNW and (i) 2 % (w/w) OPCNW

Table 3 DSC maximum of melting (T_{m1} and T_{m2}), cold crystallization temperature (T_C) and PHBV crystallinity (X_c) obtained during the first heating run, crystallization temperature (T_C) obtained from the cooling run and glass transition temperature (T_{g2}), obtained during the second heating run

	T_{m1} (°C)	ΔH_{m1} (J/g PHBV)	T_{m2} (°C)	ΔH_{m2} (J/g PHBV)	X_c (%)	T_C (°C)	T_{g2} (°C)
PHBV	135.7 ± 0.0^{a}	8.3 ± 0.2^{bc}	152.1 ± 0.4^{a}	27.3 ± 0.2^{a}	32.7 ± 0.2^{ab}	88.4 ± 0.4^{b}	-7.6 ± 0.4^{a}
1 % BCNW	136.7 ± 0.2^{ab}	6.8 ± 0.8^{ab}	152.1 ± 0.1^{a}	27.8 ± 1.0^{a}	31.7 ± 1.2^{ab}	83.6 ± 2.7^{a}	-5.7 ± 0.9^{a}
1 % WSCNW	136.4 ± 0.6^{ab}	8.1 ± 0.8^{bc}	152.2 ± 0.5^{a}	28.1 ± 1.3^{a}	33.2 ± 1.4^{ab}	86.2 ± 0.6^{ab}	-5.9 ± 0.6^{a}
1 % BGCNW	136.0 ± 0.2^{ab}	7.7 ± 0.0^{abc}	152.5 ± 0.2^{a}	30.1 ± 0.6^{a}	34.7 ± 0.4^{b}	84.9 ± 0.6^{ab}	-6.0 ± 0.0^{a}
1 % OPCNW	136.3 ± 0.8^{ab}	6.2 ± 0.7^{a}	152.2 ± 0.5^{a}	25.7 ± 0.0^{a}	29.3 ± 0.5^{a}	85.6 ± 0.1^{ab}	-6.4 ± 0.4^{a}
2 % BCNW	135.7 ± 0.2^{a}	7.3 ± 0.4^{abc}	152.5 ± 0.2^{a}	28.4 ± 2.1^{a}	32.7 ± 1.7^{ab}	85.6 ± 0.2^{ab}	-6.0 ± 0.1^{a}
2 % WSCNW	136.9 ± 0.0^{ab}	6.6 ± 0.1^{ab}	152.7 ± 0.2^{a}	27.3 ± 2.3^{a}	31.1 ± 1.6^{ab}	87.1 ± 0.4^{ab}	-7.4 ± 2.3^{a}
2 % BGCNW	137.0 ± 0.1^{ab}	8.1 ± 0.1^{bc}	152.9 ± 0.5^{a}	28.0 ± 0.0^{a}	33.1 ± 0.1^{ab}	85.0 ± 0.9^{ab}	-8.1 ± 0.0^{a}
2 % OPCNW	137.4 ± 0.7^{b}	8.7 ± 0.2^{c}	152.5 ± 0.9^{a}	28.0 ± 0.5^{a}	33.6 ± 0.5^{b}	86.5 ± 0.7^{ab}	-8.3 ± 0.3^{a}

Different superscripts within the same column indicate significant differences according to the ANOVA statistical analysis of the data ($p < 0.05$)

Table 4 TGA maximum of the weight loss first derivate (T_D) and the corresponding peak onset values and the residue at 400 °C for the PHBV films

	Onset T (°C)	T_D (°C)	Residue at 400 °C (%)
PHBV	242.9	270.7	3.6
1 % BCNW	232.5	278.7	1.2
1 % WSCNW	235.0	277.1	2.9
1 % BGCNW	231.5	267.6	2.7
1 % OPCNW	232.5	274.2	1.9
2 % BCNW	254.1	284.8	2.8
2 % WSCNW	244.3	275.4	1.9
2 % BGCNW	253.0	277.3	1.9
2 % OPCNW	246.4	274.6	1.8

PHBV due to strong hydrogen bonds established between the matrix and CNW (Yu et al. 2012). As expected, the most thermally stable BCNW (cf. Fig. 4) provided the greater thermal stability in their respective nanocomposites.

Mechanical properties

Table 5 gathers the mechanical properties of neat PHBV and the corresponding nanocomposites incorporating CNWs. From this table, it is derived that the addition of CNW did not improve the mechanical properties of PHBV, and in some cases, the presence of CNW even imposed an adverse effect on these. The nanocomposites showing the highest Young's modulus and tensile strength, without compromising their ductility, were those incorporating BCNW, whereas the most unfavorable case corresponded to the addition of OPCNW, which resulted in significantly reduced Young's modulus and tensile strength as compared to the neat PHBV. Although decreased mechanical performance of nanocomposites is usually ascribed to the lack of adhesion between the nanofiller and matrix or to the nanofiller agglomeration, these effects were not evident in the morphological characterization of the studied nanocomposites. The observed low mechanical performance of these materials may be attributed to perhaps insufficient filler-filler interactions, i.e., the absence of a network of CNW strongly interconnected within the polymeric matrix. In fact, several works have previously shown that the incorporation of unmodified CNW into hydrophobic matrixes such as PLA (Sanchez-Garcia and Lagaron 2010b), PCL (Siqueira et al. 2009) and PHBV (Martínez-Sanz et al. 2013b) by means of solution casting did not always result in improved mechanical properties, but in some cases it could even deteriorate the mechanical performance of the base material. This detrimental effect was ascribed to the fact that CNW concentrations were below the ones required for achieving the percolation threshold or simply because the CNW were agglomerated; thus,

Table 5 Young's modulus (E), tensile strength and elongation at break (ε_b) for PHBV and its nanocomposites incorporating CNW

	E (GPa)	Tensile strength (MPa)	ε_b (%)
PHBV	0.86 ± 0.09^{c}	20.08 ± 1.20^{d}	7.70 ± 0.33^{b}
1 % BCNW	0.86 ± 0.04^{c}	18.40 ± 1.07^{cd}	5.70 ± 0.56^{a}
1 % WSCNW	0.74 ± 0.05^{bc}	14.98 ± 1.28^{bc}	4.73 ± 1.32^{a}
1 % BGCNW	0.67 ± 0.11^{bc}	14.34 ± 2.24^{abc}	5.85 ± 0.46^{ab}
1 % OPCNW	0.50 ± 0.18^{ab}	12.34 ± 2.88^{ab}	5.50 ± 1.30^{a}
2 % BCNW	0.86 ± 0.10^{c}	19.36 ± 2.16^{d}	5.78 ± 0.94^{ab}
2 % WSCNW	0.52 ± 0.08^{ab}	12.36 ± 1.69^{ab}	4.73 ± 0.35^{a}
2 % BGCNW	0.63 ± 0.07^{abc}	13.41 ± 1.32^{abc}	5.12 ± 0.46^{a}
2 % OPCNW	0.40 ± 0.15^{a}	10.12 ± 2.37^{a}	4.15 ± 0.68^{a}

Different superscripts within the same column indicate significant differences according to the ANOVA statistical analysis of the data ($p < 0.05$)

their experimental aspect ratio was lower than expected. On the other hand, cellulose nanofillers with higher aspect ratios have been shown to provide a higher Young's modulus (Bras et al. 2011), probably due to the fact that lower loadings were required to reach the percolation threshold. To relate the observed mechanical properties to the morphology of the extracted CNW, their corresponding percolation threshold (υ_{RC}) was estimated from their aspect ratio by using the following equation (Oksman et al. 2006):

$$\upsilon_{RC} = \frac{0.7}{L/d}$$

In the above equation, L/d is the aspect ratio, where L is the length and d is the width or cross section. Given the densities of CNW (1.5 g/cm^3) (Gindl and Keckes 2004) and PHBV (1.2 g/cm^3) (Graupner and Müssig 2011), the percolation threshold in weight ratio was estimated as 2.6 % (w/w) for BCNW, 4.5 % (w/w) for WSCNW, 5.2 % (w/w) for BGCNW, 6.5 % (w/w) and OPCNW. Thus, the lack of improved mechanical performance may be explained by a combination of the CNW agglomeration detected for some of the nanocomposites and the low loadings used, which were below the percolation thresholds. A relatively good dispersion such as the one achieved with BCNW led to improved mechanical properties when increasing the loading from 1 % (w/w) to 2 % (w/w), thus supporting the importance of achieving the percolation threshold to maximize the mechanical performance of CNW nanocomposites. In this sense, CNW with greater aspect ratios represent an apparent advantage, since lower concentrations are required to attain optimal mechanical properties.

Water and oxygen barrier properties

Finally, the barrier properties of the developed nanocomposites were determined, and the results are summarized in Table 6. In general, the incorporation of CNW resulted in increased water permeability, whereas reduced oxygen permeability was attained for some of the samples.

As deduced from Table 6, the water permeability increase was a combination of increased water sorption and in some cases also to increased water diffusion. Similar results were observed for PHBV casting composites loaded with cellulose microfibers (Sanchez-Garcia et al. 2008) and with BCNW (Martínez-Sanz et al. 2013b), reporting minimum permeability for a loading of 1 % (w/w). Although no statistically significant differences were found for the water uptake of the various samples because of the high standard deviations, a trend of increased water sorption was observed when incorporating CNW most likely as a consequence of the presence of hydroxyl groups within cellulose. Interestingly, the samples with the smallest permeability increase, i.e., 1 % (w/w) BCNW, 1 % (w/w) WSCNW, 1 % (w/w) BGCNW and 2 % (w/w) BGCNW, were those that presented decreased water diffusion as compared to the neat PHBV. The reduced water diffusion observed in these samples may perhaps be explained by both their optimized CNW dispersion and the higher crystallinity of these CNW when compared to that of OPCNW.

Table 6 Water permeability (PH_2O) and water uptake measured at 100 % RH and estimated water diffusivity (D), and oxygen permeability (PO_2) measured at 80 % RH

	PH_2O (kg m/s m^2 Pa)	Water uptake (%)	D (m^2/s)	PO_2 (m^3 m/m^2 s Pa)
PHBV	$3.46 \pm 0.17\ e^{-15a}$	0.51 ± 0.09^a	$1.53\ e^{-12}$	$1.49 \pm 0.20\ e^{-18bc}$
1 % BCNW	$5.13 \pm 1.09\ e^{-15abcd}$	1.28 ± 0.30^a	$1.03\ e^{-12}$	$1.33 \pm 0.16\ e^{-18abc}$
1 % WSCNW	$4.71 \pm 0.70\ e^{-15abc}$	0.97 ± 0.54^a	$1.28\ e^{-12}$	$1.10 \pm 0.09\ e^{-18ab}$
1 % BGCNW	$3.65 \pm 0.88\ e^{-15ab}$	0.93 ± 0.32^a	$0.94\ e^{-12}$	$1.07 \pm 0.15\ e^{-18ab}$
1 % OPCNW	$12.03 \pm 3.48\ e^{-15abcd}$	1.55 ± 0.57^a	$2.98\ e^{-12}$	$1.46 \pm 0.20\ e^{-18bc}$
2 % BCNW	$13.41 \pm 2.40\ e^{-15d}$	1.05 ± 0.09^a	$4.84\ e^{-12}$	$1.72 \pm 0.10\ e^{-18c}$
2 % WSCNW	$12.99 \pm 4.39\ e^{-15cd}$	1.40 ± 0.50^a	$3.53\ e^{-12}$	$1.09 \pm 0.07\ e^{-18ab}$
2 % BGCNW	$3.93 \pm 0.02\ e^{-15ab}$	1.23 ± 0.45^a	$0.86\ e^{-12}$	$0.83 \pm 0.01\ e^{-18a}$
2 % OPCNW	$12.25 \pm 1.89\ e^{-15bcd}$	1.07 ± 0.13^a	$4.23\ e^{-12}$	$1.58 \pm 0.22\ e^{-18bc}$

Different superscripts within the same column indicate significant differences according to the ANOVA statistical analysis of the data ($p < 0.05$)

Regarding the oxygen barrier, permeability reductions of 26–27 and 28–44 % were detected for the nanocomposites containing 1–2 % (w/w) WSCNW and 1–2 % (w/w) BGCNW, respectively. In particular, the permeability value for the nanocomposite with 2 % (w/w) BGCNW was even lower than that reported for PHBV loaded with 5 % (w/w) nanoclay (Sanchez-Garcia and Lagaron 2010a). To the best of our knowledge, no such oxygen permeability reduction has been previously reported for PHBV nanocomposites loaded with cellulosic fillers. In agreement with the water permeability measurements, BGCNW and WSCNW seemed to be the less moisture-sensitive nanofillers; thus, they were able to preserve their oxygen blocking capacity even at high RH conditions. On the contrary, BCNW seemed to be more affected by the presence of moisture; therefore, they provided a lower barrier, especially at higher loadings. This behavior has been previously described for PHBV and PLA nanocomposites incorporating BCNW (Martínez-Sanz et al. 2012, 2013b). As reported, BCNW seem to promote the plasticization of the polymeric matrix at high RH because of the interaction of water molecules with the existing hydrogen bonds created between cellulose chains and/or with the polymeric matrix. Thus, even though BCNW were as highly dispersed as BGCNW and WSCNW, the presence of greater amounts of hydroxyl groups, which is also related to their higher specific surface area, limited their oxygen barrier performance when increasing the RH.

Conclusions

This work demonstrated that it is possible to extract CNW from food by-products by combination of a cellulose purification procedure with a subsequent hydrolysis treatment, similar to that previously optimized for the extraction of BCNW. Both BGCNW and WSCNW presented good thermal stability, crystallinity and aspect ratios, with extraction yields much higher than those reported for other food by-products.

Subsequently, the different CNW were incorporated into a commercial PHBV grade by solution casting, and the properties of the generated nanocomposites were characterized. CNW were, in general, homogeneously distributed within the PHBV matrix, although agglomeration became more noticeable when increasing the nanofiller loading. Thermal properties were not strongly affected by the addition of CNW, leading in most cases to a slightly increased thermal stability and glass transition temperature, as evidenced by TGA and DSC analyses. No mechanical improvements could be achieved, most likely because of the limited degree of dispersion achieved by the casting method and to the low CNW loadings used, which were under the estimated percolation thresholds. Interestingly, BGCNW and WSCNW presented reduced moisture sensitivity as compared with the reference BCNW, thus providing optimal barrier properties, with measurable oxygen permeability reductions spanning from 26 to 44 % as compared with pure PHBV.

Thus, BGCNW and WSCNW represent promising materials in terms of gas barrier performance to develop property-enhanced microbial nanocomposites fully derived from food by-products. Further investigation to optimize the cellulose extraction procedure, as well as to produce PHBV-CNW nanocomposites by industrial processing methods, will be required to improve the viability of these materials.

Acknowledgments Noëlle Peutat, on leave from the University of Grenoble in France, is acknowledged for her great dedication and support in the experimental work. M. Martínez-Sanz would like to thank the Spanish Ministry of Education for FPU Grant 1484. The authors acknowledge financial support from the EU FP7 ECOBIOCAP Project. The Electronic Microscopy Department in the SCIE from the University of Valencia is acknowledged for the support with SEM and TEM analyses. The Portuguese authors also acknowledge support from the FCT (Portuguese Foundation for Science and Technology) through strategic project PEst-OE/EQB/LA0023/2013.

References

Abe K, Iwamoto S, Yano H (2007) Obtaining cellulose nanofibers with a uniform width of 15 nm from wood. Biomacromolecules 8:3276–3278

Araki J, Wada M, Kuga S, Okano T (1998) Flow properties of microcrystalline cellulose suspension prepared by acid treatment of native cellulose. Colloids Surf A 142:75–82

Azizi Samir MAS, Alloin F, Dufresne A (2005) Review of recent research into cellulosic whiskers, their properties and their application in nanocomposite field. Biomacromolecules 6:612–626

Bondeson D, Mathew A, Oksman K (2006) Optimization of the isolation of nanocrystals from microcrystalline cellulose by acid hydrolysis. Cellulose 13:171–180

Bras J, Viet D, Bruzzese C, Dufresne A (2011) Correlation between stiffness of sheets prepared from cellulose whiskers and nanoparticles dimensions. Carbohydr Polym 84:211–215

Capadona JR, Shanmuganathan K, Trittschuh S, Seidel S, Rowan SJ, Weder C (2009) Polymer nanocomposites with nanowhiskers isolated from microcrystalline cellulose. Biomacromolecules 10:712–716

Delmer DP, Amor Y (1995) Cellulose biosynthesis. Plant Cell 7:987–1000

Elanthikkal S, Gopalakrishnapanicker U, Varghese S, Guthrie JT (2010) Cellulose microfibres produced from banana plant wastes: isolation and characterization. Carbohydr Polym 80:852–859

French AD (2014) Idealized powder diffraction patterns for cellulose polymorphs. Cellulose 21:885–896

Garrido L, Jiménez I, Ellis G, Cano P, García-Martínez JM, López L, De La Peña E (2011) Characterization of surface-modified polyalkanoate films for biomedical applications. J Appl Polym Sci 119:3286–3296

Gindl W, Keckes J (2004) Tensile properties of cellulose acetate butyrate composites reinforced with bacterial cellulose. Compos Sci Technol 64:2407–2413

Graupner N, Müssig J (2011) A comparison of the mechanical characteristics of kenaf and lyocell fibre reinforced poly(lactic acid) (PLA) and poly(3-hydroxybutyrate) (PHB) composites. Compos Part A Appl Sci 42:2010–2019

Helbert W, Cavaillé JY, Dufresne A (1996) Thermoplastic nanocomposites filled with wheat straw cellulose whiskers. Part I: processing and mechanical behavior. Polym Compos 17:604–611

Iguchi M, Yamanaka S, Budhiono A (2000) Bacterial cellulose—a masterpiece of nature's arts. J Mater Sci 35:261–270

Jiang L, Morelius E, Zhang J, Wolcott M, Holbery J (2008) Study of the poly(3-hydroxybutyrate-co-3-hydroxyvalerate)/cellulose nanowhisker composites prepared by solution casting and melt processing. J Compos Mater 42:2629–2645

Kargarzadeh H, Ahmad I, Abdullah I, Dufresne A, Zainudin SY, Sheltami RM (2012) Effects of hydrolysis conditions on the morphology, crystallinity, and thermal stability of cellulose nanocrystals extracted from kenaf bast fibers. Cellulose 19:855–866

Lu P, Hsieh YL (2012) Preparation and characterization of cellulose nanocrystals from rice straw. Carbohydr Polym 87:564–573

Lu H, Gui Y, Zheng L, Liu X (2013) Morphological, crystalline, thermal and physicochemical properties of cellulose nanocrystals obtained from sweet potato residue. Food Res Int 50:121–128

Martínez-Sanz M, Lopez-Rubio A, Lagaron J (2011a) Optimization of the nanofabrication by acid hydrolysis of bacterial cellulose nanowhiskers. Carbohydr Polym 85:228–236

Martínez-Sanz M, Olsson RT, Lopez-Rubio A, Lagaron JM (2011b) Development of electrospun EVOH fibres reinforced with bacterial cellulose nanowhiskers. Part I: characterization and method optimization. Cellulose 18:335–347

Martínez-Sanz M, Lopez-Rubio A, Lagaron JM (2012) Optimization of the dispersion of unmodified bacterial cellulose nanowhiskers into polylactide via melt compounding to significantly enhance barrier and mechanical properties. Biomacromolecules 13:3887–3899

Martínez-Sanz M, Lopez-Rubio A, Lagaron JM (2013a) Nanocomposites of ethylene vinyl alcohol copolymer with thermally resistant cellulose nanowhiskers by melt compounding (I): morphology and thermal properties. J Appl Polym Sci 128:2666–2678

Martínez-Sanz M et al (2013b) Characterization of polyhydroxyalkanoates synthesized from microbial mixed cultures and of their nanobiocomposites with bacterial cellulose nanowhiskers. New Biotechnol 31:364–376

Martínez-Sanz M, Lopez-Rubio A, Fabra MJ, Lagaron JM (2014) A new method for developing industrially viable nanocrystalline cellulose-based nanocomposites via melt compounding. J Renew Mater 2:107–117

MontañoLeyva B, Ghizzi D, Da Silva G, Gastaldi E, Torres-Chávez P, Gontard N, Angellier-Coussy H (2013) Biocomposites from wheat proteins and fibers: structure/

mechanical properties relationships. Ind Crop Prod 43:545–555

Montaño-Leyva B, Rodriguez-Felix F, Torres-Chávez P, Ramirez-Wong B, López-Cervantes J, Sanchez-Machado D (2011) Preparation and characterization of durum wheat (Triticum durum) straw cellulose nanofibers by electrospinning. J Agric Food Chem 59:870–875

Morais JPS, Rosa MF, de Souza Filho MM, Nascimento LD, do Nascimento DM, Cassales AR (2013) Extraction and characterization of nanocellulose structures from raw cotton linter. Carbohydr Polym 91:229–235

Mussatto SI (2014) Brewer's spent grain: a valuable feedstock for industrial applications. J Sci Food Agric 94:1264–1275

Oh SY, Yoo DI, Shin Y, Seo G (2005) FTIR analysis of cellulose treated with sodium hydroxide and carbon dioxide. Carbohydr Res 340:417–428

Oksman K, Mathew AP, Bondeson D, Kvien I (2006) Manufacturing process of cellulose whiskers/polylactic acid nanocomposites. Compos Sci Technol 66:2776–2784

Pires EJ, Ruiz HA, Teixeira JA, Vicente AA (2012) A new approach on Brewer's spent grains treatment and potential use as lignocellulosic yeast cells carriers. J Agric Food Chem 60:5994–5999

Rahimi M, Behrooz R (2011) Effect of cellulose characteristic and hydrolyze conditions on morphology and size of nanocrystal cellulose extracted from wheat straw. Int J Polym Mater Polym Biomater 60:529–541

Ramos P et al (2013) Valorization of olive mill residues: antioxidant and breast cancer antiproliferative activities of hydroxytyrosol-rich extracts derived from olive oil by-products. J Ind Crop Prod 46:359–368

Rånby BG (1949) Aqueous colloidal solutions of cellulose micelles. Acta Chem Scand 3:649–650

Rosa MF et al (2010) Cellulose nanowhiskers from coconut husk fibers: effect of preparation conditions on their thermal and morphological behavior. Carbohydr Polym 81:83–92

Sanchez-Garcia MD, Lagaron JM (2010a) Novel clay-based nanobiocomposites of biopolyesters with synergistic barrier to UV light, gas, and vapour. J Appl Polym Sci 118:188–199

Sanchez-Garcia MD, Lagaron JM (2010b) On the use of plant cellulose nanowhiskers to enhance the barrier properties of polylactic acid. Cellulose 17:987–1004

Sanchez-Garcia MD, Gimenez E, Lagaron JM (2008) Morphology and barrier properties of solvent cast composites of thermoplastic biopolymers and purified cellulose fibers. Carbohydr Polym 71:235–244

Sanchez-Silva L, López-González D, Villaseñor J, Sánchez P, Valverde JL (2012) Thermogravimetric-mass spectrometric analysis of lignocellulosic and marine biomass pyrolysis. Bioresour Technol 109:163–172

Satyamurthy P, Jain P, Balasubramanya RH, Vigneshwaran N (2011) Preparation and characterization of cellulose nanowhiskers from cotton fibres by controlled microbial hydrolysis. Carbohydr Polym 83:122–129

Scandola M et al (1997) Polymer blends of natural poly(3-hydroxybutyrate-co-3-hydroxyvalerate) and a synthetic atactic poly(3-hydroxybutyrate). Characterization and biodegradation studies. Macromolecules 30:2568–2574

Silva GGD, Couturier M, Berrin JG, Buléon A, Rouau X (2012) Effects of grinding processes on enzymatic degradation of wheat straw. Bioresour Technol 103:192–200

Siqueira G, Bras J, Dufresne A (2009) Cellulose whiskers versus microfibrils: influence of the nature of the nanoparticle and its surface functionalization on the thermal and mechanical properties of nanocomposites. Biomacromolecules 10:425–432

Sugiyama J, Persson J, Chanzy H (1991) Combined infrared and electron diffraction study of the polymorphism of native celluloses. Macromolecules 24:2461–2466

Sun JX, Sun XF, Zhao H, Sun RC (2004) Isolation and characterization of cellulose from sugarcane bagasse. Polym Degrad Stab 84:331–339

Sun XF, Xu F, Sun RC, Fowler P, Baird MS (2005) Characteristics of degraded cellulose obtained from steam-exploded wheat straw. Carbohydr Res 340:97–106

Ten E, Turtle J, Bahr D, Jiang L, Wolcott M (2010) Thermal and mechanical properties of poly(3-hydroxybutyrate-co-3-hydroxyvalerate)/cellulose nanowhiskers composites. Polymer 51:2652–2660

Ten E, Bahr DF, Li B, Jiang L, Wolcott MP (2012) Effects of cellulose nanowhiskers on mechanical, dielectric, and rheological properties of poly(3-hydroxybutyrate-co-3-hydroxyvalerate)/cellulose nanowhisker composites. Ind Eng Chem Res 51:2941–2951

Wang N, Ding E, Cheng R (2007) Thermal degradation behaviors of spherical cellulose nanocrystals with sulfate groups. Polymer 48:3486–3493

Watanabe K, Tabuchi M, Morinaga Y, Yoshinaga F (1998) Structural features and properties of bacterial cellulose produced in agitated culture. Cellulose 5:187–200

Yu HY, Qin ZY, Liu YN, Chen L, Liu N, Zhou Z (2012) Simultaneous improvement of mechanical properties and thermal stability of bacterial polyester by cellulose nanocrystals. Carbohydr Polym 89:971–978